Available online at www.sciencedirect.com
ScienceDirect
Journal of the European Ceramic Society 28 (2008) 1279–1285
www.elsevier.com/locate/jeurceramsoc

Mechanical and physical behavior of spark plasma sintered ZrC–ZrB_2–SiC composites

Shu-Qi Guo [a,*], Yutaka Kagawa [a,b], Toshiyuki Nishimura [c], Dowhan Chung [d], Jenn-Ming Yang [d]

[a] *Composites and Coating Center, National Institute for Materials Science, 1-2-1 Sengen, Tsukuba, Ibaraki 305-0047, Japan*
[b] *Research Center for Advanced Science and Technology, The University of Tokyo, 4-6-1 Komaba, Meguro-ku, Tokyo 153-8505, Japan*
[c] *Nano Ceramic Center, National Institute for Materials Science, 1-1 Namiki, Tsukuba, Ibaraki 305-0044, Japan*
[d] *Department of Materials Science and Engineering, University of California, Los Angeles, CA 900095-1595, USA*

Received 20 May 2007; received in revised form 9 August 2007; accepted 19 August 2007
Available online 22 October 2007

Abstract

The effects of compositions on mechanical, thermal and electrical properties of ZrC–ZrB_2–SiC composites were examined. The composites were consolidated by spark plasma sintering. The elastic moduli of the composites were measured using the longitudinal and transverse soundwave velocities measured, whereas the hardness and fracture toughness of the composites were determined using an indentation measurement. The results indicated that the shear modulus was in the range 180–225 GPa and the Young's modulus is in the range 435–517 GPa. The ranges of hardness and fracture toughness values were measured to be 18.8–21.5 GPa, and 4.6–6.1 MPa $m^{1/2}$, respectively. On the other hand, the thermal and electrical conductivities of the ZrC–ZrB_2–SiC composites were measured at room temperature by a nanoflash technique and a current–voltage method, respectively. The thermal conductivities for the composites were in the range 38.25–92.85 W m^{-1} K^{-1}. The electrical conductivities of the composites were in the range 0.916–4.521 × 10^4 $(\Omega\,cm)^{-1}$.

Keywords: ZrC; ZrB_2; SiC; Spark plasma sintering; Mechanical properties; Thermal conductivity; Electrical conductivity

1. Introduction

Diborides and carbides of zirconium (ZrB_2 and ZrC) have extremely high melting point (>3000 °C), high thermal and electrical conductivities, chemical inertness against molten metals, and great thermal shock resistance.[1–4] The unique combinations of mechanical and physical properties make them attractive candidates for structural applications at ultra-high temperatures. However, the use of those single-phase ceramics materials for high-temperature structural applications is limited by their poor oxidation, thermal shock and ablation resistance as well as poor damage tolerance. Composite approach has been successfully adopted in order to improve the oxidation and ablation resistance of single-phase ceramics. For example, the addition of second phase such as SiC to ZrB_2 results in a composite with improvement of strength, better oxidation, thermal shock and ablation resistance.[5–8] The improvement of oxidation and ablation resistance is believed to arise from the formation of coherent passivating oxide scale on the surface. More recently, the ZrC–ZrB_2–SiC multiphase composite system has been demonstrated to have superior resistance to ablation or conversion than do the corresponding ZrB_2/SiC composites under arc-jet environment.[8] The ZrB_2–30ZrC–10SiC (v/o %) composites have been successfully consolidated using both hot-pressing and spark plasma sintering.[9,10] Furthermore, this composite exhibited high strength with low scattering of strength up to 1500 °C as well as these components are both thermodynamically and chemically stable at high temperature because the intergranular reaction in the composite was absent.[10] However, the effect of separate components on mechanical, thermal and electrical properties of ZrB_2–ZiC–SiC composites are not systematically studied yet. The compositional dependence of these properties is very important for designing ZrB_2–ZrC–SiC composites in sustained thermomechanical applications.

On the other hand, spark plasma sintering (SPS) is one of the most recent processing techniques developed for densifying ceramic materials, including poorly sinterable compounds.[11,12] One advantage of SPS concerning ceramics is that the grain

* Corresponding author. Tel.: +81 29 859 2223; fax: +81 29 859 2401.
E-mail address: GUO.Shuqi@nims.go.jp (S.-Q. Guo).

0955-2219/$ – see front matter © 2007 Elsevier Ltd. All rights reserved.
doi:10.1016/j.jeurceramsoc.2007.08.009

growth of starting materials is restricted, as a considerable shorter sintering time (within several minutes) is required compared to hot-pressing or hot isostatic pressing, thereby retaining the fine and homogenous grains. Other is to enhance densification of poorly sinterable ceramics, as a result of the spark discharge generated between powders as well as the presence of the electrical field under pulsed direct current. Previous studies in ZrB_2-based ceramic materials showed that SPS enhanced densification and refined microstructure in very short processing cycles.[10,13] This is attributable to the presence of the electrical field during SPS which caused faster diffusion due to the enhanced migration speed of ions.[14]

In the present study, ZrC–ZrB_2–SiC composites with different compositions were consolidated by spark plasma sintering. The elastic moduli of composites were calculated using the longitudinal and transverse soundwave velocities measured. The fracture toughness was determined using an indentation crack size measurement. Thermal and electrical properties of the composites were investigated at room temperature by a nanoflash technique and a current–voltage method, respectively. Correlations between compositions and properties were examined.

2. Experimental procedure

2.1. Materials

The starting powders used in this study were ZrB_2 (Grade F, Japan New Metals, Tokyo, Japan), average particle size ≈2.12 μm, ZrC (Grade F, Japan New Metals), average particle size ≈2.32 μm; and α-SiC (Grade UF-15, H.C. Starck, Berlin, Germany), average particle size ≈0.5 μm. In order to examine the effects of composition on the mechanical, thermal and electrical properties, eight ZrC–ZrB_2–SiC compositions were prepared in this study. These compositions are shown in Table 1. The powder mixtures were wet mixed using SiC milling media and ethanol for 24 h, and then dried in an oven. Before sintering, the dried mixtures were sieved through a metallic sieve with –60-mesh screen size. The powder mixture was put into a graphite die lines with graphite foil and densified using spark plasma sintering (SPS-1030, Sumitomo Coal Mining Co. Ltd., Tokyo, Japan). The sintering was performed at 1950 °C for 2 min under an external pressure of 50 MPa in argon atmosphere. The temperature of the sample was automatically raised to 600 °C, and then was monitored by an optical pyrometer through a hole opened in the die and automatically regulated to the final sintering temperature with heating rate of ∼400 °C/min. The pressure was applied at room temperature and held constant until the end of the sintering cycle. The load was removed when the die temperature dropped below 1000 °C with the cooling rate of ∼600 °C/min. During the entire sintering process, the changes in the height of the samples with temperature along the pressing direction were recorded to monitor the densification behavior. The final sintered specimen size was 10 mm in diameter pellets with a thickness of ∼3.0 mm. After removing the surface of the sintered compact, the density of the sintered composite compacts was measured from Archimedes method with distilled water as medium. The sintered composite pellets were then polished with a diamond paste up to 1.0 μm. The morphology of the composites was characterized by field emission scanning electron microscopy (FE-SEM, S-4800, Hitachi High-Technologies Corporation, Tokyo, Japan), and the crystalline phases were identified by X-ray diffractometry (XRD, JDX-3500, Japan Electron Optocs Laboratory Co. Ltd., JEOL, Tokyo, Japan).

2.2. Elastic moduli and fracture toughness measurements

The elastic moduli measurements of the composites were performed using an ultrasonic technique (TDS 3052B, Tektronix Inc., Beaverton, OR USA) with a fundamental frequency of 20 MHz. Young's modulus (E), shear modulus (G) and Poisson's ratio (ν) were calculated using the longitudinal and transverse soundwave velocities measured in the composite specimens. The details of calculations are reported elsewhere.[15] The hardness and fracture toughness, K_{IC}, of the composites were determined using an indentation technique. The indentation tests were performed on the polished surface of the specimens by loading with a Vickers microhardness indenter (AVK-A, Akashi Co. Ltd., Yokohama, Japan) for 15 s in ambient air at room temperature. The corresponding diagonals of the indentation and crack sizes were measured using an optical microscope attached to an indenter. The indentation load of 98 N was used, and 10 indents were made for each measurement. The fracture toughness, K_{IC}, of composites were calculated from the Anstis equation.[16]

2.3. Thermal and electrical conductivity measurements

The thermal diffusivity, α, of the composites was measured on a disk-shaped specimen with a diameter of 10 mm and thick-

Table 1
Compositions, densities and relative densities, and elastic constant of the ZrC–ZrB_2–SiC composites consolidated by SPS

Materials	Compositions (mol%)			Theoretical density (g/cm^3)	True density (g/cm^3)	Relative density (%TD)	Elastic properties		
	ZrB_2	ZrC	SiC				G (GPa)	E (GPa)	ν
ZZS-1	33.3	33.3	33.3	5.51	5.44	98.7	205	477	0.17
ZZS-2	70	15	15	5.85	5.76	98.5	225	517	0.16
ZZS-3	15	70	15	6.14	6.05	98.5	180	435	0.18
ZZS-4	15	55	30	5.70	5.65	99.1	192	449	0.17
ZZS-5	30	20	50	5.01	4.94	98.6	206	486	0.18
ZZS-6	55	15	30	5.51	5.44	98.7	215	500	0.16
ZZS-7	55	30	15	5.93	5.86	98.8	211	496	0.18
ZZS-8	30	55	15	6.06	5.97	98.5	196	457	0.17

ness of ~2 mm using the nanoflash technique (LFA447/2-4N, Nanoflash, NETZSCH-Geratebau GmbH, Postfach, Germany). The flash source is a xenon flash lamp operating in the wavelength range of 0.15–2 μm. Prior to the measurements, the samples were coated with a colloidal graphite spray in order to enhance the absorption of the xenon light pulse energy and the emission of IR radiation to the temperature detector. Also, the heat capacity, C_p, was measured with alumina as the reference material. All of the measurements were performed in ambient air at room temperature. The accuracy of the thermal diffusivity measurements was ±3%, and the specific heat accuracy is ±5%. Subsequently, the thermal conductivity of the composites, k_c, is determined from thermal diffusivity, α, heat capacity, C_p, and true density, ρ, of the composites according to the following equation[17]:

$$k_c = \rho C_p \alpha \quad (1)$$

Moreover, the electrical conductivity measurements of the composites were performed using the standard four-point probe method at room temperature to reduce the effects of contact resistance. A power supply (Model: 6220, Keithley, Cleveland, OH, USA) and digital multimeter (Model: 2182 Nanovoltmeter, Keithley) were used to measure the *IV* characteristics of the samples.

3. Results and discussion

3.1. Densification and microstructure

Some shrinkage curves obtained during the SPS cycle for the ZrC–ZrB_2–SiC composite materials consolidated by SPS are shown in Fig. 1. The shrinkage behavior of ZrC–ZrB_2–SiC (ZZS) is similar for the studied compositions, regardless of the component contents. The measurable shrinkage was observed at temperatures ranging from 1500 to 1600 °C, depending upon the compositions. It was found that the reduction of ZrB_2 amount lowered the onset temperature of densification. However, this temperature is insensitive to the amount of ZrC and/or SiC in the studied compositions. For examples, the onset temperature of densification was determined to be ~1530 °C for ZZS-1, ~1580 °C for ZZS-2, ~1550 °C for ZZS-3, and ~1540 °C for ZZS-5. During subsequent densification, all of the compositions showed almost the same shrinkage rate with time. The main part of the densification occurred within a period of ~2 min, whereas conventional hot press typically required hours (>1 h) of densification at substantially higher temperatures (>2000 °C) to yield fully densified compacts. The measured densities and relative densities for the ZrC–ZrB_2–SiC composition materials consolidated by SPS are summarized in Table 1. The theoretical densities of the composites were calculated according to the rule of mixtures. It is evident that all the composites were almost fully densified (relative density >98%) and their relative density was almost the same, regardless of compositions. This is attributed to the fact that the same shrinkage behavior was observed during SPS for all the studied compositions.

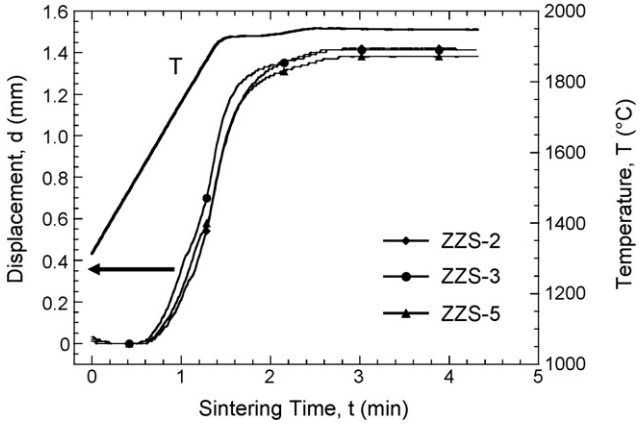

Fig. 1. Some typical examples of recorded shrinkage curves during the SPS cycle for the ZrC–ZrB_2–SiC composites consolidated by SPS.

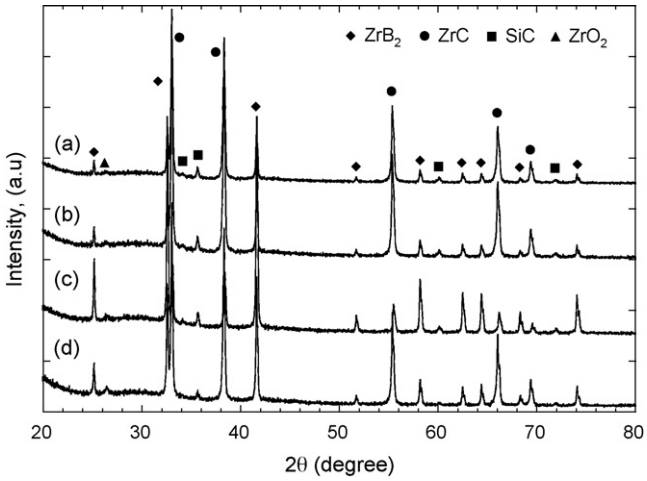

Fig. 2. Examples of X-ray diffraction patterns for the ZrC–ZrB_2–SiC composites consolidated by spark plasma sintering: (a) ZZS-2, (b) ZZS-4, (c) ZZS-6 and (d) ZZS-8.

Some examples of X-ray diffraction patterns for the ZrC–ZrB_2–SiC composite materials consolidated by SPS are presented in Fig. 2. Although the peaks of ZrB_2, ZrC and SiC phases showed the different intensity with compositions, the primary crystalline phases of ZrB_2, ZrC and SiC were detected in every case, and a trace of ZrO_2 phase was also present. This trace of ZrO_2 phase is mostly due to the oxide layer on the surfaces of the starting ZrC powders. Typical microstructural features of the ZrC–ZrB_2–SiC composites were observed under FE-SEM, some examples are shown in Fig. 3. The general microstructures of the ZrC–ZrB_2–SiC composites are similar, consisting of the equiaxed ZrB_2 (grey contrast), ZrC (bright contrast), and SiC (dark contrast) grains. In the case of ZZS-1, ZrB_2, ZrC, and SiC particles are homogenously present in the composite (Fig. 3(a)) because the added ZrB_2, ZrC, and SiC amounts are the same for this composition. For other compositions, however, the primary component in the composite, such as ZrB_2 particles for ZZS-2, ZZS-6, and ZZS-7 (Fig. 3(d)), ZrC particles for ZZS-3, ZZS-4, ZZS-8 (Fig. 3(b)), SiC particles for ZZS-5 (Fig. 3(c)), formed some blocks with the other two components homogenously dispersed in it. In addition, the intergranular reaction

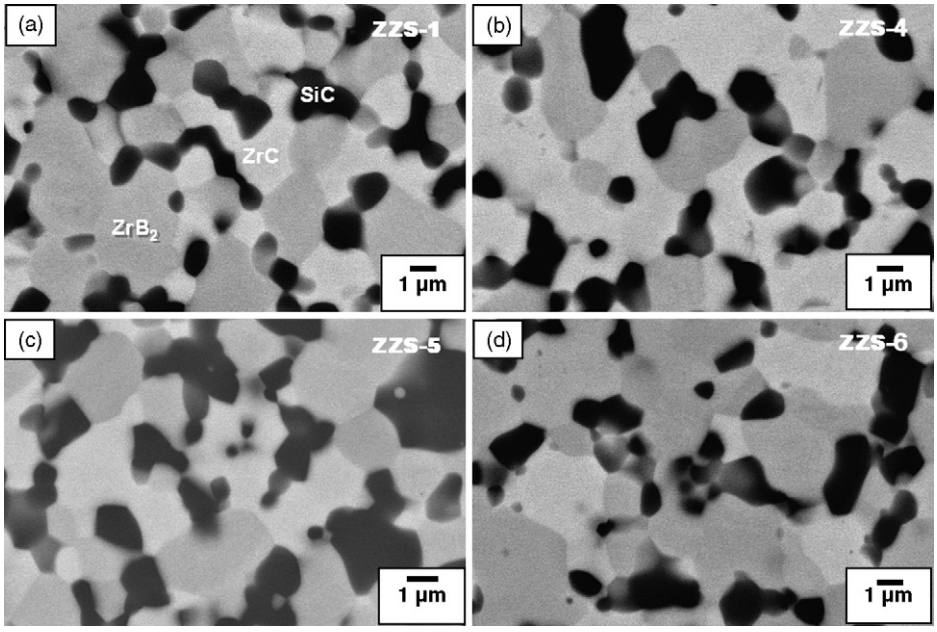

Fig. 3. Typical examples of FE-SEM images for the ZrC–ZrB_2–SiC composites consolidated by SPS.

among these components was not observed at least with the FE-SEM resolution for any case.

3.2. Elastic moduli, hardness and fracture toughness

The elastic moduli measured in the various ZrC–ZrB_2–SiC compositions consolidated by SPS are listed in Table 1. From this table, it is found that the shear and Young's moduli related to component content. In the case of the same amount of ZrB_2-, ZrC-, and SiC-containing composition (ZZS-1), the shear and Young's moduli are 205 and 477 GPa, respectively. Then, both the elastic moduli increased with increasing ZrB_2 as well as SiC addition, but decreased with increasing ZrC addition. The highest shear and Young's moduli were measured in the ZZS-2 composition, and their values are 225 and 517 GPa, respectively. The lowest shear and Young's moduli were measured in the ZZS-3 composition, and their values are 180 and 435 GPa, respectively. In contrast, Poisson's ratio remains almost the constant for the studied compositions regardless of component content.

The hardness and fracture toughness of the ZrC–ZrB_2–SiC composites obtained from an indentation technique are summarized in Table 2. Note that for the ZZS-5 composition the fracture toughness was not listed in the table because it is difficult to measure the crack length accurately. The ranges of hardness and fracture toughness values were measured to be 18.8–21.5 GPa, and 4.6–6.1 MPa $m^{1/2}$, respectively. The results indicated that both the hardness and fracture toughness of the composites are dependent on the compositions. The compositional dependence of hardness and fracture toughness may be associated with the complex residual stress state that develops during cooling from the processing temperature due to the thermal expansion mismatch among ZrB_2 (CTE: 6.5 ppm/°C), ZrC (CTE: 7.1 ppm/°C) and SiC (CTE: 4.7 ppm/°C). A typical cracking pattern is shown in Fig. 4. The crack propagated across the ZrC, ZrB_2 and SiC grains without being deflected along the grain boundaries. The fracture toughness of hot-pressed ZrB_2, SiC was reported to be 2.3–3.1 MPa $m^{1/2}$,[18] and 3.0–4.3 MPa $m^{1/2}$,[19] respectively.

Table 2
Hardness and fracture toughness of the ZrC–ZrB_2–SiC composites consolidated by SPS

Materials	Hardness, H (MPa)	Fracture toughness, K_{IC} (MPa $m^{1/2}$)
ZZS-1	19.1 ± 0.9	6.1 ± 0.7
ZZS-2	21.5 ± 1.3	6.0 ± 0.5
ZZS-3	19.5 ± 1.0	4.6 ± 0.2
ZZS-4	18.8 ± 0.7	5.5 ± 0.3
ZZS-5	20.4 ± 1.9	–
ZZS-6	19.6 ± 0.7	5.7 ± 0.4
ZZS-7	19.4 ± 1.2	5.0 ± 0.3
ZZS-8	19.6 ± 0.7	5.6 ± 0.2

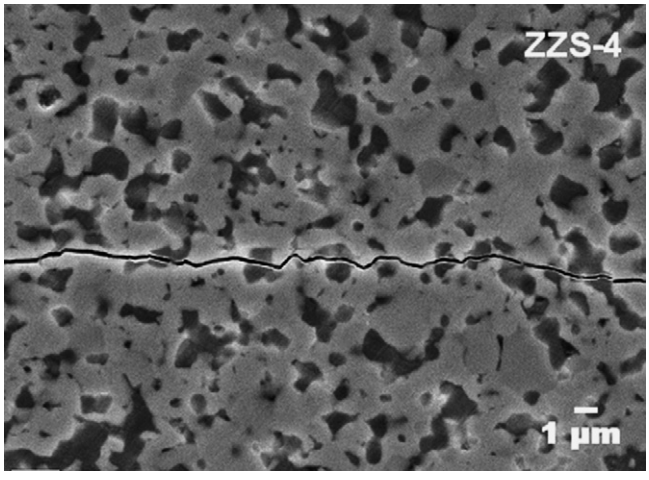

Fig. 4. Typical cracking behavior of ZrC–ZrB_2–SiC composites consolidated by SPS.

The fracture toughness values of ZrB_2–SiC (10–30% SiC) composites were reported to be between 4.1 and 5.3 MPa $m^{1/2}$.[8] Therefore, the fracture toughness values of the ZrC–ZrB_2–SiC multiple composites are comparable to that of the single-phase ceramics and ZrB_2–SiC composites.

3.3. Thermal conductivity

The measured heat capacities, thermal diffusivities, and the calculated thermal conductivities of the ZrC–ZrB_2–SiC composites consolidated by SPS are summarized in Table 3. From this table, it is obvious that the heat capacity and the thermal diffusivity decreased with increasing ZrC amount, but increased with increasing SiC and ZrB_2 additions. The heat capacity was in the range of 0.50–0.62 J g^{-1} K^{-1}, showing a compositional dependence. The thermal diffusivity is the range of 12.36–30.46 mm^2 s^{-1}. It is evident that the compositional dependence is stronger for the thermal diffusivity than for the heat capacity. This strong dependence of thermal diffusivity suggests that the thermal conductivity of the ZrC–ZrB_2–SiC composition is dominated by the heat flow in the composites. In the case of ZZS-1, the same amount of ZrB_2-, ZrC-, and SiC-containing composition, the thermal conductivity measured was 72.64 W m^{-1} K^{-1}. The thermal conductivity then decreased with increasing amount of ZrC. In particular, the ZZS-3 composition, 70 vol.% ZrC-containing composition, showed the low heat capacity as well as the lowest thermal diffusivity, in turn resulting in the lowest thermal conductivity in the studied compositions. The thermal conductivity dropped from 72.64 W m^{-1} K^{-1} for the ZZS-1 composition to 38.25 W m^{-1} K^{-1} for the ZZS-3 composition for approximate loss of 50%. On the other hand, the thermal conductivity of the ZrC–ZrB_2–SiC composites is higher with increasing ZrB_2 as well as of SiC amount. The improvement of thermal conductivity is more substantial for increasing SiC amount than for increasing ZrB_2 amount. The ZZS-5 composition, 50 vol.% SiC-containing composite, showed the highest heat capacity as well as the highest thermal diffusivity, which in turn resulting in the highest thermal conductivity among all the composition materials. The thermal conductivity increased from 72.64 W m^{-1} K^{-1} for the ZZS-1 composite to 92.85 W m^{-1} K^{-1} for the ZZS-5 composition material for approximate increase of 30%.

Table 3
Thermal properties measured at room temperature for the ZrC–ZrB_2–SiC composites consolidated by SPS

Materials	Heat capacity, C_p (J g^{-1} K^{-1})	Thermal diffusivity,α (mm^2 s^{-1})	Thermal conductivity, k_c (W m^{-1} K^{-1})
ZZS-1	0.58	22.98	72.64
ZZS-2	0.54	27.69	85.63
ZZS-3	0.51	12.36	38.25
ZZS-4	0.55	16.82	51.77
ZZS-5	0.62	30.46	92.85
ZZS-6	0.58	28.20	89.02
ZZS-7	0.53	23.64	73.73
ZZS-8	0.50	16.33	49.07

It is known that the thermal conductivity of the composites is dependent on the thermal conductivity of the components and the interfacial thermal resistance between the components. The thermal conductivity of SiC is higher than that of both the ZrB_2 and ZrC materials,[1,20,21] and ZrC has the lowest thermal conductivity among the ZrB_2, ZrC, and SiC components.[1,20] This implies that the increasing SiC and ZrB_2 content should improve thermal conductivity of ZrC–ZrB_2–SiC ceramics. Conversely, increasing ZrC content should lead to decrease in thermal conductivity. This effect is closely linked to the amount of SiC, ZrB_2 and ZrC additions as well as to the distribution because they influence the heat flow resistance through the components and the interfaces. In the case of high ZrC-containing ZrC–ZrB_2–SiC (ZZS-3, ZZS-4, and ZZS-8), the ZrC is the pristine phase and other two phases (ZrB_2 and SiC) were dispersed in it (Fig. 3(b)). This structure characteristics led to increase resistance for the heat flow through the components and their interfaces, compared to ZZS-1. This thermal resistance was enhanced with increasing amount of ZrC. In the case of high SiC or ZrB_2-containing ZrC–ZrB_2–SiC (ZZS-2, ZZS-5, ZZS-6, and ZZS-7), on the other hand, the ZrC particles were embedded in SiC or ZrB_2 matrix (Fig. 3(c) and (d)). This characteristics structure of SiC or ZrB_2 particles formed in ZrC–ZrB_2–SiC composites should enhance its heat transport capability because it could provide a route of higher heat flow. In particular, SiC has the highest thermal conductivity among ZrB_2, SiC and ZrC. Thus, in the present study, the addition of SiC or ZrB_2 improved heat capacity as well as heat transport, resulting in high thermal conductivity.

3.4. Electrical conductivity

In Fig. 5, examples of the current–voltage relations measured at room temperature for two ZrC–ZrB_2–SiC composites are presented. It is clear that the current increased linearly with voltage, i.e. a linear relationship between current and voltage. This indicated that good Ohmic contacts have been realized between the measured composite samples and the electrode. Additionally, the slope of current–voltage curve is related

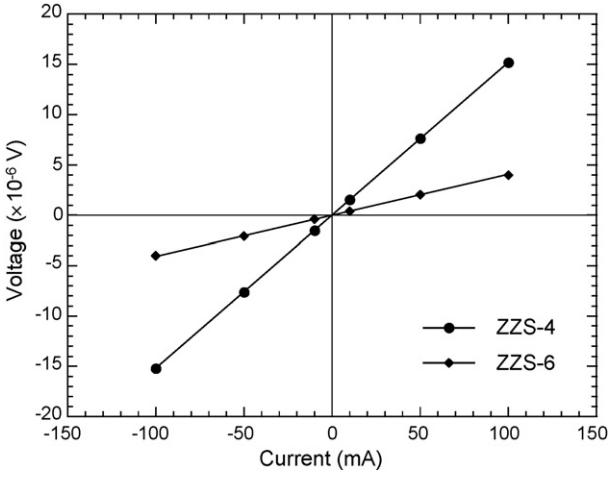

Fig. 5. Some examples of current versus voltage measured at room temperature for the ZrC–ZrB_2–SiC composites consolidated by SPS.

Table 4
Electrical properties measured at room temperature for the ZrC–ZrB_2–SiC composites consolidated by SPS

Materials	Electrical resistivity, R ($\times 10^{-5}\ \Omega$ cm)	Electrical conductivity ($\times 10^4\ \Omega^{-1}\ cm^{-1}$)
ZZS-1	6.226	1.606
ZZS-2	2.212	4.521
ZZS-3	9.384	1.066
ZZS-4	10.917	0.916
ZZS-5	8.282	1.207
ZZS-6	3.333	3.002
ZZS-7	3.094	3.231
ZZS-8	5.682	1.760

with the compositions: high ZrB_2 content resulted in a lower slope, while high ZrC resulted in a high slope. This indicated that the resistance decreased with increasing the ZrB_2 addition in the ZrC–ZrB_2–SiC compositions. The measured electrical resistivity and conductivity of the ZrC–ZrB_2–SiC composites consolidated by SPS are summarized in Table 4. The electrical conductivity of the ZrC–ZrB_2–SiC composites were measure to be in the range of 0.916–4.521 $\times 10^4$ $(\Omega\,cm)^{-1}$. In the case of ZZS-1, 33.3 vol.% ZrB_2–33.3 vol.% ZrC–33.3 vol.% SiC composites, the measured electrical conductivity was $1.606 \times 10^4\ \Omega^{-1}\ cm^{-1}$. The electrical conductivity was then improved with ZrB_2 addition. The highest electrical conductivity was measured in the ZZS-2 composition composite and the value was $4.521 \times 10^4\ \Omega^{-1}\ cm^{-1}$. On the other hand, the electrical conductivity decreased with increasing ZrC and/or SiC contents. The lowest electrical conductivity was measured in the ZZS-4 composition material. Although ZrB_2 and ZrC are located in the electrical conductivity range of conductors, the electrical conductivity of ZrC was significantly lower than that of ZrB_2.[20] Thus, the decrease in electrical conductivity due to ZrC addition is a result of the lower electrical conductivity of ZrC. In addition, it was found that the addition of SiC further reduced the electrical conductivity of the ZrC–ZrB_2–SiC composites because SiC is a semiconductor. However, the lowest electrical conductivity was not observed in the 50 vol.% SiC-containing composites, but in the 30 vol.% SiC-containing composite. This is because of high ZrB_2 content for the former (30 vol.% ZrB_2) compared with the latter (15 vol.% ZrB_2). This indicated that ZrB_2 addition is important for improving the electrical conductivity of ZrC–ZrB_2–SiC composites. Although the high ZrC and/or SiC-containing ZrC–ZrB_2–SiC composites exhibited lower electrical conductivity as compared with to high ZrB_2-containing composites, the electrical conductivities of all the ZrC–ZrB_2–SiC composites investigated in this study are still within the range of conductors. As a result, electrical discharge machining can be used for all the ZrC–ZrB_2–SiC composites.

4. Conclusions

(1) The ZrC–ZrB_2–SiC composites were consolidated by SPS at 1950 °C for 2 min under a pressure of 50 MPa, and the composites were almost the fully densed regardless of compositions. The microstructure of the composites consisted of the equiaxed ZrB_2, ZrC and SiC grains. The other secondary phases were homogenously dispersed in the matrix consisting of a primary component phase.

(2) The shear modulus of the ZrC–ZrB_2–SiC composites were in the range 180–225 GPa, and the Young's modulus was in the range 435–517 GPa, depending on compositions. Poisson's ratio was almost the same for all the studied compositions. The ranges of hardness and fracture toughness values were measured to be 18.8–21.5 GPa, and 4.6–6.1 MPa $m^{1/2}$, respectively.

(3) The thermal conductivity of the ZrC–ZrB_2–SiC composites decreases with increasing ZrC content, but it increases with increasing SiC and/or ZrB_2 content. The measured thermal conductivities are in the range 38.25–92.85 $W\,m^{-1}\,K^{-1}$, depending on component content.

(4) The electrical conductivities of the ZrC–ZrB_2–SiC composites increased with increasing ZrB_2 content, conversely, the electrical conductivity decreased with increasing SiC and/or ZrC content. The measured electrical conductivities were in the range 0.916–4.521 $\times 10^4$ $(\Omega\,cm)^{-1}$.

References

1. Kuwabara, K., Some characteristics and applications of ZrB_2 ceramics. *Bull. Ceram. Soc. Jpn.*, 2002, **37**(4), 267–271.
2. Upadhya, K., Yang, J.-M. and Hoffmann, W. P., Materials for ultrahigh temperature structural applications. *Am. Ceram. Soc. Bull.*, 1997, **76**(12), 51–56.
3. Guo, S. Q., Nishimura, T., Kagawa, Y. and Tanaka, H., Thermal and electric properties in hot-pressed ZrB_2–$MoSi_2$–SiC composites. *J. Am. Ceram. Soc.*, 2007, **90**(7), 2255–2258.
4. Kida, O. and Segawa, Y., ZrB_2 composite sintered materials, US Patent 4,636,481, 1987.
5. Bull, J., White, J. and Kaufman, L., Ablation resistant zirconium and hafnium ceramics, US Patent 5,750,450, 1998.
6. Brown, A. S., Hypersonic designs with a sharp edge. *Aerospace Am.*, 1997, **35**(9), 20–21.
7. Mroz, C., Zirconium diboride. *Am. Ceram. Soc. Bull.*, 1994, **73**(6), 141–142.
8. Norasetthekul, S., Eubank, P. T., Bradley, W. L., Bozkurt, B. and Stucker, B., Use of zirconium diboride-copper as an electrode in plasma applications. *J. Mater. Sci.*, 1999, **34**(6), 1261–1270.
9. Medri, V., Monteverde, F., Balbo, A. and Bellosi, A., Comparison of ZrB_2–ZrC–SiC composites fabricated by spark plasma sintering and hot-pressing. *Adv. Eng. Mater.*, 2005, **7**(3), 159–163.
10. Bellosi, A., Monteverde, F. and Sciti, D., Fast densification of ultra-high-temperature ceramics by spark plasma sintering. *Int. J. Appl. Ceram. Technol.*, 2006, **3**(1), 32–40.
11. Nygren, M. and Shen, Z., On the preparation of bio-, nano- and structural ceramics and composites by spark plasma sintering. *Solid State Sci.*, 2003, **5**, 125–131.
12. Nygren, M. and Shen, Z., Novel assemblies via spark plasma sintering. *Silic. Ind.*, 2004, **69**, 211–218.
13. Medri, V., Monteverde, F., Balbo, A. and Bellosi, A., Comparison of ZrB_2–ZrC–SiC composites fabricated by spark plasma sintering and hot-pressing. *Adv. Eng. Sci.*, 2005, **7**, 159–163.
14. Khor, K. A., Cheng, K. H., Yu, L. G. and Boey, F., Thermal conductivity and dielectric constant of spark plasma sintered aluminum nitride. *Mater. Sci. Eng. A*, 2003, **347**, 300–305.
15. Guo, S. Q., Hirosaki, N., Yamamoto, Y., Nishimura, T. and Mitomo, M., Hot-press sintering silicon nitride with Lu_2O_3 addition: elastic moduli and fracture toughness. *J. Eur. Ceram. Soc.*, 2003, **23**, 537–545.
16. Anstis, G. R., Chantikul, P., Lawn, B. R. and Marshall, D. B., A critical evaluation of indentation techniques for measuring fracture tough-

ness. I. Direct crack measurements. *J. Am. Ceram. Soc.*, 1981, **64**(9), 533–538.
17. Parker, W. J., Jenkins, W. J., Butler, C. P. and Abbott, G. L., Flash method of determining thermal diffusivity, heat capacity and thermal conductivity. *J. Appl. Phys.*, 1961, **32**(9), 1679–1684.
18. Monteverde, F. and Bellosi, A., Beneficial effects of AlN as sintering aid on microstructure and mechanical properties of hot-pressed ZrB_2. *Adv. Eng. Mater.*, 2003, **5**(7), 508–512.
19. Tanaka, H. and Zhou, Y., Low temperature sintering and elongated grain growth of 6H–SiC powder with AlB_2 and C additives. *J. Mater. Res.*, 1999, **14**(2), 518–522.
20. *Manufactures Data*. Japan New Metals Corporation Ltd., Tokyo, Japan (http://www.jnm.co.jp).
21. Takeda, Y., Development of high-thermal-conductive SiC ceramics. *Am. Ceram. Soc. Bull.*, 1988, **67**(12), 1961–1963.